MICROBIOLOGY

Monoclonal antibodies targeting the FimH adhesin protect against uropathogenic *E. coli* UTI

Edward D. B. Lopatto[1,2]†, Jesús M. Santiago-Borges[1,2,3]†, Denise A. Sanick[1,2], Sameer Kumar Malladi[4], Philippe N. Azimzadeh[1,2], Morgan W. Timm[1,2], Isabella F. Fox[4,5], Aaron J. Schmitz[4], Jackson S. Turner[4], Shaza M. Sayed Ahmed[4], Lillian Ortinau[1,2,3], Nathaniel C. Gualberto[1,2], Jerome S. Pinkner[1,2], Karen W. Dodson[1,2], Ali H. Ellebedy[1,4,6]*, Andrew L. Kau[1,2,3]*, Scott J. Hultgren[1,2,6]*

As antimicrobial resistance increases, urinary tract infections (UTIs) are expected to pose an increased burden in morbidity and expense on the health care system, increasing the need for alternative antibiotic-sparing treatments. Most UTIs are caused by uropathogenic *Escherichia coli* (UPEC), whereas *Klebsiella pneumoniae* causes a large portion of non-UPEC UTIs. Both bacteria express type 1 pili tipped with the mannose-binding FimH adhesin critical for UTI pathogenesis. We generated and biochemically characterized 33 murine monoclonal antibodies (mAbs) to FimH. Three mAbs protected mice from *E. coli* UTI. Mechanistically, we show that this protection is Fc independent and mediated by the ability of these mAbs to sterically block FimH function by recognizing a high-affinity FimH conformation. Our data reveal that FimH mAbs hold promise as an antibiotic-sparing treatment strategy.

INTRODUCTION

Urinary tract infections (UTIs) affect over 400 million individuals worldwide yearly (*1*, *2*), leading to $2.8 billion in health care and productivity-related costs annually in the US alone (*3*). Around 25% of individuals will suffer from recurrent UTIs, which severely impairs their quality of life (*4*). Furthermore, 27% of all sepsis cases can be traced to urinary origin (*5*). This is aggravated by the increased prevalence of multidrug-resistant uropathogens (*6*), such as uropathogenic *Escherichia coli* (UPEC), responsible for 70 to 90% of UTIs, and *Klebsiella pneumoniae*, one of the most prevalent non-UPEC uropathogens (*7*–*9*). UTIs represent the fourth leading cause of death attributed to or associated with antibiotic resistance (*10*). Thus, developing antibiotic-sparing strategies to prevent UTIs caused by these difficult-to-treat uropathogens is crucial. One promising approach for new antibacterial treatments is to neutralize key extracellular adhesins to prevent bacterial colonization and invasion into tissue and biofilm formation.

UPEC and *K. pneumoniae* express chaperone-usher pathway (CUP) type 1 pili that are tipped with the mannose-binding FimH adhesin essential in (i) bladder colonization, (ii) ascension to cause pyelonephritis, (iii) invasion into terminally differentiated umbrella cells of the bladder, (iv) the formation of intracellular biofilms in luminal bladder cells, and (v) causing an epigenetic imprint in the bladder that predisposes to recurrent UTI (*11*–*18*). FimH is a two-domain protein with an N-terminal lectin domain containing a deep binding pocket that recognizes mannose with stereochemical specificity (*19*) and a C-terminal pilin domain linking the adhesin to the pilus. At the tip of the assembled type 1 pilus, FimH exists in a conformational equilibrium between a high-affinity relaxed state and a low-affinity tense state controlled by structural interactions between the FimH lectin and pilin domains (*20*). In the high-affinity relaxed state, the FimH lectin domain is highly mobile with respect to the pilin domain. In contrast, in the low-affinity tense state, the pilin domain constrains the lectin domain and allosterically deforms the mannose-binding pocket. UPEC FimH occupies both tense and relaxed conformations, whereas the equilibrium in the highly invariant and conserved *K. pneumoniae* FimH is primarily shifted toward the tense low-binding conformation, explaining its poor mannose-binding properties despite an identical mannose-binding site (*21*).

A vaccine against UPEC FimCH has revealed an 73% reduction in recurrent UTIs caused by UPEC or *Klebsiella* spp. in a phase 1A/1B clinical trial, showing potential to prevent the two most common UTI pathogens with a FimH targeted therapeutic (*22*, *23*). The effectiveness of FimH vaccination is associated with antibody responses that inhibit FimH binding (*24*, *25*). Here, we characterized monoclonal antibodies (mAbs) from mice immunized with *E. coli* and *K. pneumoniae* FimH lectin domains and found cross-reactive antibodies that bind to four distinct FimH structural epitopes (Classes 1 to 4), which block FimH binding in vitro. Using cryo–electron microscopy (cryo-EM), we found that the mAbs are selectively bound to the epitopes displayed in the high-affinity relaxed conformation of FimH. Using binding studies and mouse UTI models, we identified Class 1 mAbs that blocked FimH binding to mannose through steric interference leading to protection against UPEC in mouse UTI models. From structure to an antibiotic alternative therapeutic, these results guide future optimization of FimH mAbs and vaccination strategies to treat *E. coli* and *K. pneumoniae* UTIs, two of the most prominent uropathogens with increasing antibiotic resistance.

[1]Department of Molecular Microbiology, Washington University in St. Louis, St. Louis, MO, USA. [2]Center for Women's Infectious Disease Research, Washington University in St. Louis, St. Louis, MO, USA. [3]Division of Allergy and Immunology, Department of Medicine, Washington University in St Louis, St Louis, MO, USA. [4]Department of Pathology and Immunology, Washington University School of Medicine, St Louis, MO, USA. [5]Henry M. Jackson Foundation for the Advancement of Military Medicine, Bethesda, MD, USA. [6]Center for Vaccines and Immunity to Microbial Pathogens, Washington University School of Medicine, St. Louis, MO, USA.
*Corresponding author. Email: ellebedy@wustl.edu (A.H.E.); akau@wustl.edu (A.L.K.); hultgren@wustl.edu (S.J.H.)
†These authors contributed equally to this work.

RESULTS

$FimH_{LD}$ mAbs can cross-react with *E. coli* and *K. pneumoniae* FimH

Female C57BL/6J mice were immunized with the lectin domain truncates of FimH ($FimH_{LD}$) from either *E. coli* (UTI89) or *K. pneumoniae* (TOP52). Heavy chain V-D-J and light chain V-J fragments from sorted plasmablasts isolated from draining lymph nodes were cloned into human IgG expression vectors to create chimeric murine/human mAbs as previously described (*26*). In total, 33 clonally distinct mAbs were generated from *E. coli* (8 mAbs) and *K. pneumoniae* (25 mAbs) that bound the respective $FimH_{LD}$ (referred to as Ec and Kp mAbs, respectively). The $FimH_{LD}$ structures of *E. coli* and *K. pneumoniae* are highly homologous [root mean square deviation (RMSD) = 0.420] with an 86% amino acid sequence identity, including an identical binding pocket (Fig. 1, A and B, and fig. S1). By enzyme-linked immunosorbent assay (ELISA), most mAbs bound to their respective $FimH_{LD}$ antigen with half-maximal effective binding concentrations (EC_{50}) ranging from 8 to 50 ng/ml, whereas some bound more weakly with EC_{50} values from 50 to 751 ng/ml (Fig. 1D). Half (4 of 8) of the Ec mAbs also reacted with *K. pneumoniae* $FimH_{LD}$, and 80% (20 of

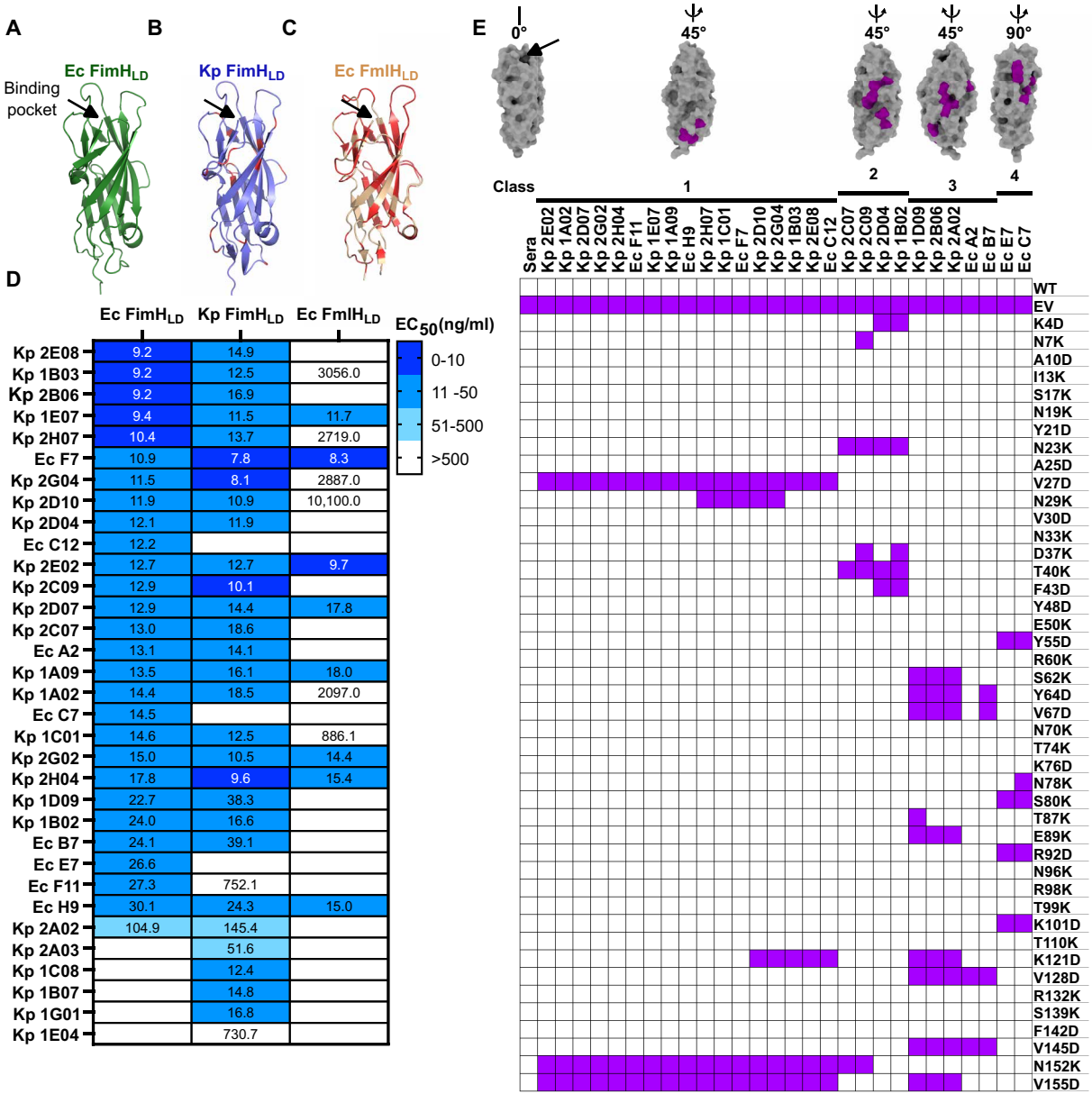

Fig. 1. FimH mAbs bind to four distinct epitope classes. Structures of (**A**) *E. coli* $FimH_{LD}$ (PDB 1KLF), (**B**) *K. pneumoniae* $FimH_{LD}$ (PDB 9AT9), and (**C**) *E. coli* $FmlH_{LD}$ (PDB 6AOW). Residue differences from *E. coli* $FimH_{LD}$ are highlighted in red. (**D**) ELISA EC_{50} values for each mAb to the listed protein. White cells with no values indicate EC_{50} values were above the range measured in the assay. (**E**) Epitope mapping of mAbs (top labels) to a panel of FimH mutants (right labels). Binding classes were determined by shared residues that abrogated mAb binding, which are highlighted in purple in the table (bottom). Epitope residues representing a majority of mAbs within an epitope class are colored in purple on the surface of *E. coli* $FimH_{LD}$ (top) (PDB 1KLF). Black arrows on structures indicate the binding pocket.

25) of Kp mAbs reacted with *E. coli* $FimH_{LD}$. Furthermore, eight mAbs (two Ec and six Kp mAbs) that reacted with both FimH antigens also bound with high affinity to a third structurally similar (RMSD = 0.699 to Ec FimH) *E. coli* adhesin, FmlH lectin domain ($FmlH_{LD}$), an adhesin that binds to exposed galactose residues on bladder tissue during chronic cystitis infections (*27*) (Fig. 1, C and D, and fig. S1).

$FimH_{LD}$ mAbs bind diverse epitopes

To determine the structural regions of $FimH_{LD}$ that were recognized by each mAb, we generated a mutant library consisting of 44 surface-exposed mutations to bulky charged residues across the lectin domain of full-length *E. coli* FimH. Binding of the mAbs to the stable mutant FimH proteins was determined by ELISA, which revealed four binding site classes (Fig. 1E; structural regions of FimH are defined in fig. S1 and table S1). Class 1 mAbs (4 Ec and 13 Kp mAbs), bind with high affinity to both *E. coli* and *K. pneumoniae* $FimH_{LD}$ and $FmlH_{LD}$. Class 1 mAbs were unable to bind *E. coli* FimH Class 1 epitope residue mutants V27D, N152K, and V155D located in the insertion and swing loops and in the part of the linker between the pilin and receptor binding domains, suggesting that they bind to the base of the lectin domain. Class 2 mAbs (four Kp mAbs) bound to *E. coli* and *K. pneumoniae* $FimH_{LD}$ but did not react with $FmlH_{LD}$, consistent with the sequence differences between *E. coli* $FimH_{LD}$ and *E. coli* $FmlH_{LD}$ (fig. S1). Class 2 mAbs shared the inability to bind to the Class 2 epitope residue mutants N23K and T40K in *E. coli* FimH, suggesting that they bind to the side of the $FimH_{LD}$ body between the base of the binding clamp loop and basal swing loop. A majority of Class 3 mAbs (two Ec mAbs and three Kp mAbs) bound to both *E. coli* and *K. pneumoniae* $FimH_{LD}$ but not to $FmlH_{LD}$. Class 3 mAbs were unable to bind to Class 3 epitope residue mutants S62K, Y64D, V67D, E89K, K121D, V128D, V145D, and V155D in *E. coli* FimH, suggesting that they bind below the binding pocket to the opposite lateral side of the $FimH_{LD}$ body from the Class 2 epitope, covering regions on β sheet B below the clamp loop and peripheral α helix. Class 4 mAbs (two Ec mAbs) were only able to bind *E. coli* $FimH_{LD}$ and not to *K. pneumoniae* $FimH_{LD}$ or *E. coli* $FmlH_{LD}$ and were unable to bind to Class 4 epitope residue mutants Y55D, S80K, R92D, and K101D in *E. coli* FimH, suggesting that they bound at the base of binding loop two and backside of $FimH_{LD}$. Five Kp mAbs were not mapped as they did not bind *E. coli* FimH. Thus, immunization of *E. coli* and *K. pneumoniae* $FimH_{LD}$ antigens generated mAbs bound to four unique surfaces (Class 1 to 4 epitopes) on *E. coli* FimH. Below, mAb nomenclature denotes the epitope class recognized by the mAb after the Ec or Kp designation. Kp $FimH_{LD}$ mAbs whose epitopes could not be determined are left unnumbered.

Structural basis of FimH mAb recognition

The structural basis of Class 1 to 3 mAbs binding to $FimH_{LD}$ was determined by cryo-EM of FimCH complexed with fragment antigen-binding regions (Fabs) of Kp1 2H04, Ec1 F7, Kp2 2C07, and Ec3 B7 (Fig. 2 and figs. S2 to S4). In each case, we identified density corresponding to the Fab-$FimH_{LD}$ complex; however, because of the inter-domain flexibility of FimH in the relaxed state, we were unable to detect the density of the FimH pilin domain and FimC chaperone. The observed interaction between $FimH_{LD}$ and Fabs confirmed and extended the epitope mapping described above. The structural basis of Kp1 2H04 Fab and Ec1 F7 Fab binding to Class 1 epitope of FimH revealed that they both interacted with the $FimH_{LD}$ swing loop and linker regions (Class 1 epitope residues A24 to N29 and N151 to T158) and coordinated multiple aromatic residues around $FimH_{LD}$ Class 1 residue P26 (Fig. 2, A to C, F, G, and J, and fig. S4). However, Kp1 2H04 and Ec1 F7 Fabs bound to the *E. coli* $FimH_{LD}$ at differing angles. Ec1 F7 Fab was rotated ~20° relative to Kp1 2H04 Fab bound to $FimH_{LD}$ (Fig. 2C and fig. S4). The structure of the Class 2 Kp2 2C07 Fab-$FimH_{LD}$ complex revealed strong binding to the Class 2 epitope residues Y21 to A27 and N151 to D153 (Fig. 2, D and H). Class 3 Ec3 B7 Fab bound to β sheet B of *E. coli* FimH including Class 3 residue Y64 (Fig. 2, I and K), which has been identified as a "toggle switch" between tense and relaxed FimH conformation, with the residue undergoing a major solvent-accessible surface area change in the conformational transition (*28*). This binding mode suggests a role of our Class 3 mAbs specifically binding and stabilizing the relaxed FimH conformation as mutagenesis of Class 3 residue Y64 abolished Class 3 mAb binding in the epitope mapping (Fig. 1E). Together, the high-resolution cryo-EM structures identified critical FimH interactions of the mAb epitope classes.

$FimH_{LD}$ mAbs bind preferentially to the relaxed conformation

When FimH is incorporated at the tip of type 1 pili, the receptor binding domain samples a conformational equilibrium between low-affinity tense and high-affinity relaxed conformations (fig. S1). The identified mAb binding epitopes of $FimH_{LD}$, particularly Classes 1 to 3, are in regions that vary extensively between tense and relaxed conformational states (*29*) (fig. S1 and table S1). Thus, we investigated whether the conformational dynamics influence the epitopes recognized by Class 1 to 4 mAbs by measuring binding to FimH-tipped piliated *E. coli* bacteria using ELISA. Class 1 mAbs displayed the highest reactivity, whereas Class 2 to 4 mAbs displayed greatly diminished reactivity to FimH tipped type 1 pili of *E. coli* (Fig. 3A). Thus, we tested Class 1 to 4 mAbs against *E. coli* expressing conformational FimH variants. A majority of mAbs from Classes 1 to 4 had increased binding to the relax-shifted A27V/V163A *E. coli* FimH mutant tipping type 1 pili and very weak binding to the tense-shifted A62S *E. coli* FimH mutant, despite similar levels of type 1 pili expression as measured by Western blot (Fig. 3B and fig. S5). To investigate binding of the highest affinity Class 1 and 2 mAbs to FimH in a tip-like state, we used biolayer interferometry (BLI) to measure binding to recombinant FimH. We prepared "tip-like" recombinant full-length FimH by incubating *E. coli* FimCH with the N-terminal extension (Nte) peptide of FimG resulting in a donor strand exchange reaction where the FimG Nte displaces the FimC chaperone to produce *E. coli* $FimG_{nte}H$ complex that samples dynamic conformations like that of FimH tipping type 1 pili (*20*). Class 1 and 2 mAbs had varied binding affinity to *E. coli* $FimG_{nte}H$, with k_{on} rates lower than binding to *E. coli* $FimH_{LD}$ (k_{on} rates between 2×10^4 to 1×10^5 M^{-1} s^{-1}) (Fig. 3, C and D, and figs. S6 and S7). This finding indicated that Class 1 and 2 mAbs had a binding preference for the relaxed FimH conformation likely due to $FimH_{LD}$ being the immunizing antigen. Allosteric lectin-pilin domain interactions are necessary for formation of the tense conformation (*20*). Thus, the $FimH_{LD}$ truncate, which lacks a pilin domain, is primarily in the relaxed conformation.

$FimH_{LD}$ mAbs inhibit FimH mannosylated protein binding

The structural analysis showed mAbs recognizing epitopes near the mannose-binding pocket, suggesting that mAbs may interfere with

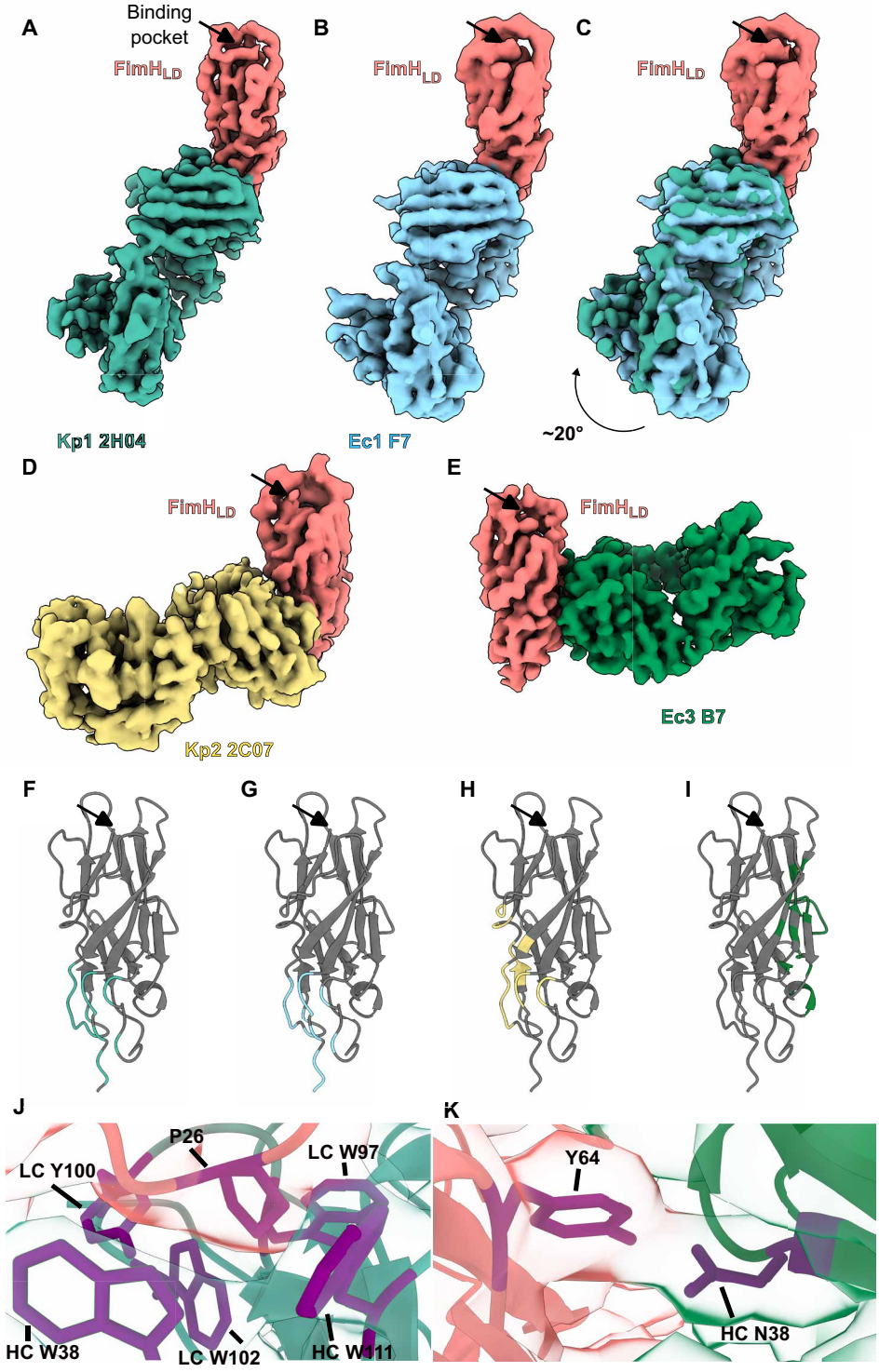

Fig. 2. Structural basis of FimH mAb protection. (**A** to **E**) Cryo-EM density maps of Fabs bound to FimH$_{LD}$. (A) Kp1 2H04 (teal), (B) Ec1 F7 (cyan), (C) Kp1 2H04 and Ec1 F7 maps superimposed on each other, (D) Kp2 2C07 (sand), and (E) Ec3 B7 (dark green) bound to FimH$_{LD}$ (salmon). (**F** to **I**) Binding epitopes of the Fabs on FimH$_{LD}$ colored by the same color scheme as (A) to (E). Density map overlaid on model residue interactions of (**J**) Kp1 2H04 (cyan) with FimH P26 and (**K**) Ec3 B7 (dark green) with FimH Y64. mAb heavy chain residues are labeled "HC," and light chain residues are labeled "LC." Black arrows on structures indicate the FimH mannose-binding pocket.

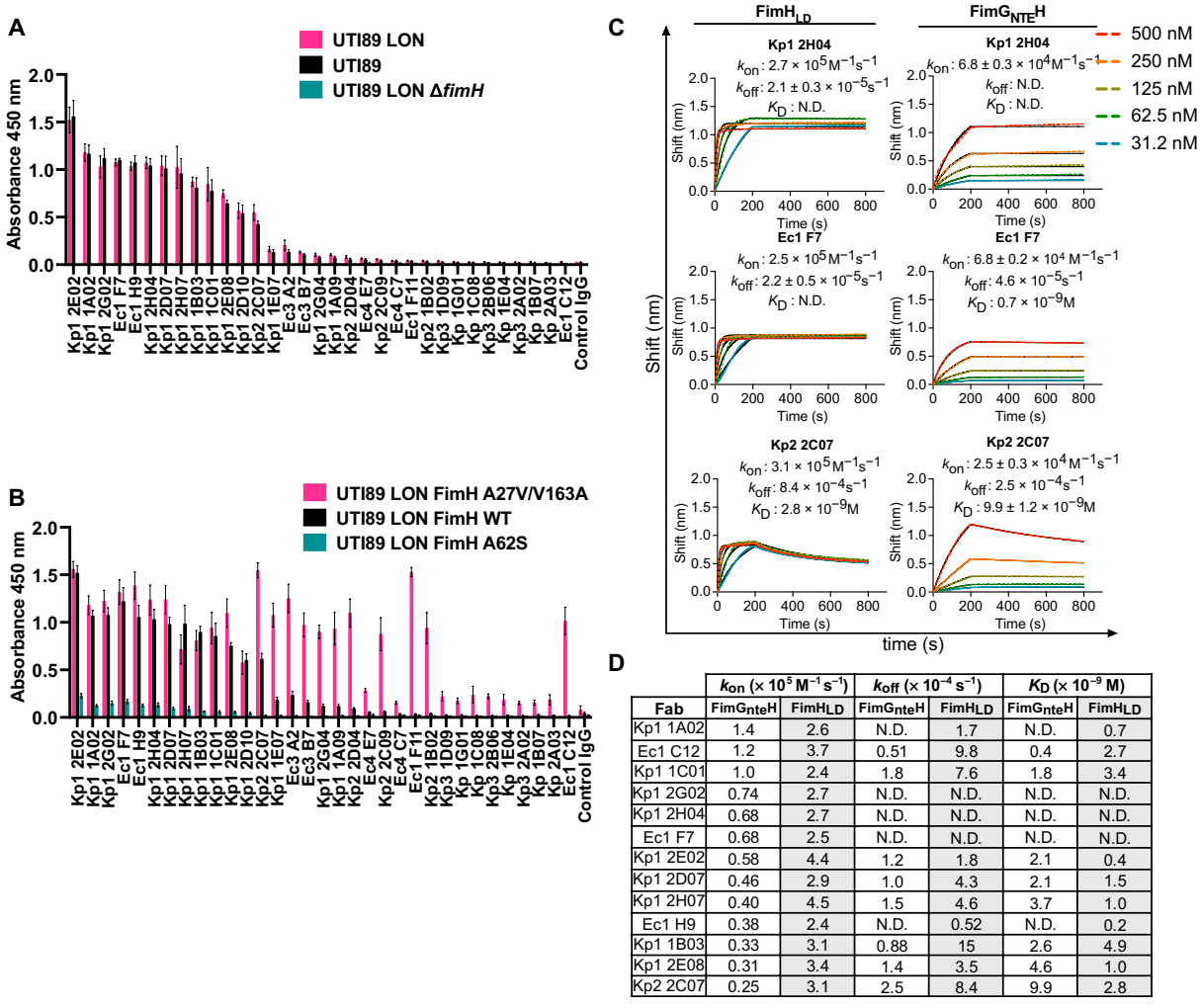

Fab	k_{on} ($\times 10^5$ M^{-1} s^{-1})		k_{off} ($\times 10^{-4}$ s^{-1})		K_D ($\times 10^{-9}$ M)	
	$FimG_{nte}H$	$FimH_{LD}$	$FimG_{nte}H$	$FimH_{LD}$	$FimG_{nte}H$	$FimH_{LD}$
Kp1 1A02	1.4	2.6	N.D.	1.7	N.D.	0.7
Ec1 C12	1.2	3.7	0.51	9.8	0.4	2.7
Kp1 1C01	1.0	2.4	1.8	7.6	1.8	3.4
Kp1 2G02	0.74	2.7	N.D.	N.D.	N.D.	N.D.
Kp1 2H04	0.68	2.7	N.D.	N.D.	N.D.	N.D.
Ec1 F7	0.68	2.5	N.D.	N.D.	N.D.	N.D.
Kp1 2E02	0.58	4.4	1.2	1.8	2.1	0.4
Kp1 2D07	0.46	2.9	1.0	4.3	2.1	1.5
Kp1 2H07	0.40	4.5	1.5	4.6	3.7	1.0
Ec1 H9	0.38	2.4	N.D.	0.52	N.D.	0.2
Kp1 1B03	0.33	3.1	0.88	15	2.6	4.9
Kp1 2E08	0.31	3.4	1.4	3.5	4.6	1.0
Kp2 2C07	0.25	3.1	2.5	8.4	9.9	2.8

Fig. 3. mAbs bind the relaxed conformation of FimH. FimH mAb binding to (**A**) UTI89 bacteria and (**B**) UTI89 overexpressing conformationally shifted FimH variants ($n = 3$; error bars represent SEM). (**C**) Representative binding curves of Kp1 2H04, Ec1 F7, and Kp2 2C07 Fab binding $FimH_{LD}$ and $FimG_{NTE}H$. Results are from kinetic measurements of dilution series of one experiment. (**D**) Observed BLI binding kinetics to Ec $FimG_{NTE}H$ and Ec $FimH_{LD}$. N.D. means not determined due to the off rate being below the detection limit.

FimH binding. Thus, $FimH_{LD}$ mAbs were tested for their ability to block *E. coli* and *K. pneumoniae* $FimH_{LD}$ binding to highly mannosylated glycoprotein bovine submaxillary mucin (BSM). At a 5:1 molar ratio of mAb to $FimH_{LD}$, assays measuring mAbs that inhibit binding to BSM in ELISAs ranged from no inhibition to 85% inhibition compared to untreated control (Fig. 4A). Only eight mAbs (representing epitope Classes 1 to 3) inhibited both $FimH_{LD}$ proteins at greater than 50% at a 5:1 molar ratio. We selected mAbs from Classes 1 to 3 from both *E. coli* and *K. pneumoniae* antigens with the highest inhibition to $FimH_{LD}$ and the strongest binding to FimH tipping type 1 pili on the surface of bacteria to test for the ability to inhibit mannose-dependent *E. coli* bacterial hemagglutination of guinea pig erythrocytes. When present in high concentrations (17 μM), we found that all mAbs tested can inhibit hemagglutination with more potency than α-D-mannopyranoside. However, the FimH mAbs displayed greatly variable inhibition potency with 50% inhibition concentration ranging from 700 nM to above 17 μM (Fig. 4B). We selected Kp1 2H04 to further test for ability to block $FimH_{LD}$ binding to mouse bladder tissue as Kp1 2H04 had high inhibition in the FimH BSM ELISA and *E. coli* hemagglutination. At a 10:1 molar ratio of mAb to $FimH_{LD}$ protein, Ec $FimH_{LD}$ and Kp $FimH_{LD}$ mixed with control IgG bound strongly to the bladder epithelial cells. However, Kp1 2H04 mAb treatment completely blocked Ec $FimH_{LD}$ and Kp $FimH_{LD}$ binding to mouse bladder tissue (Fig. 4, C and D).

$FimH_{LD}$ mAbs protect against UTI

To determine the ability of the mAbs to prevent UTI, we screened eight mAbs in a prophylactic model. We chose Class 1 to 3 mAbs Ec1 F7, Kp1 2H04, Kp1 1A02, Kp1 2E02, Kp1 1B03, Kp1 2E08 mAbs, Kp2 2C07, and Ec3 B7 mAb for these assays because they bind with high-affinity to tip-like FimH, inhibit bacterial *E. coli* FimH binding, and represent three epitope classes from *E. coli* and *K. pneumoniae* FimH antigens. Each mAb was administered via intraperitoneal injection at 0.5 mg per mouse 24 hours before infection with *E. coli* UTI89. Bladder and kidney titers were enumerated 24 hours postinfection

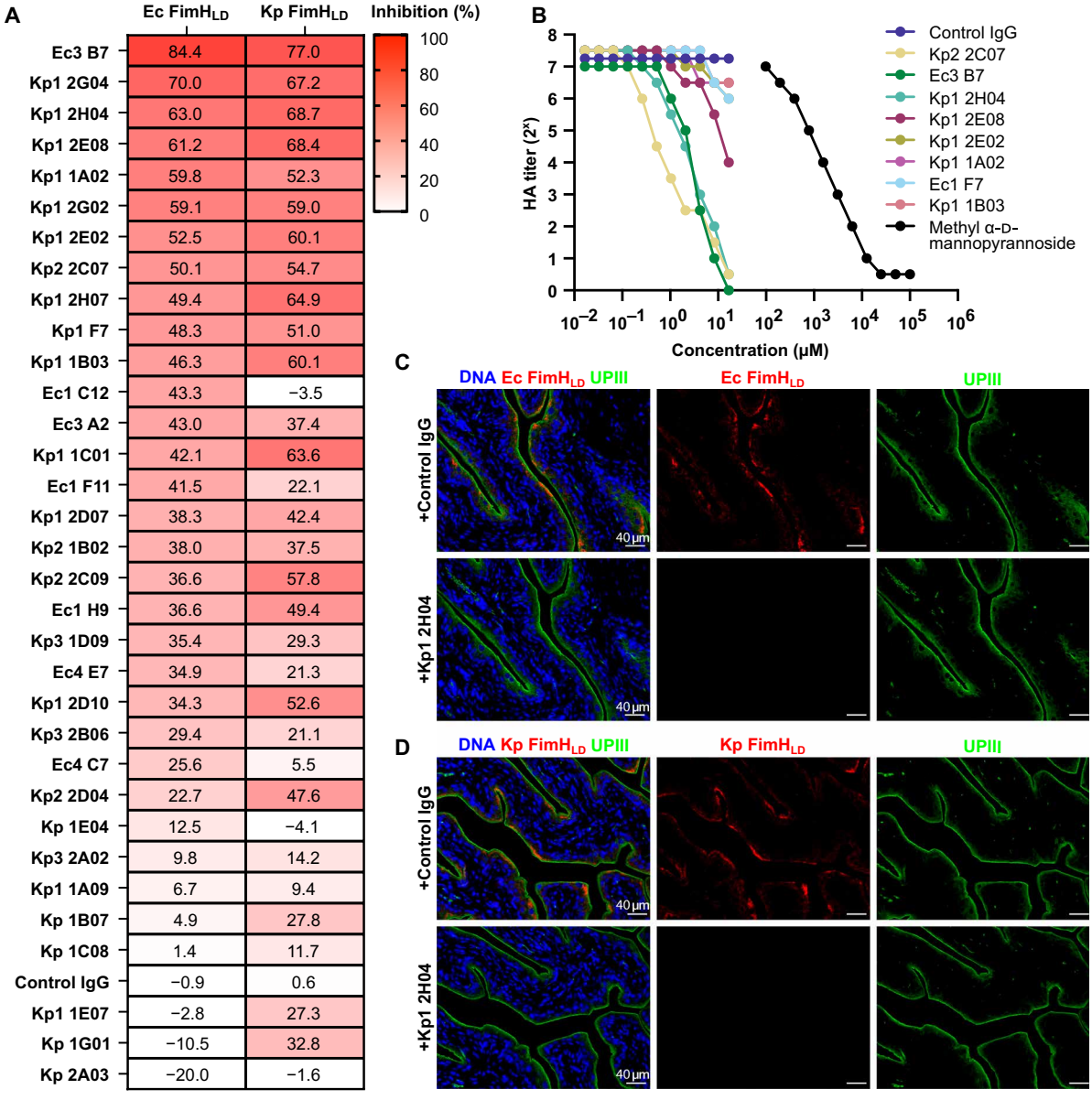

Fig. 4. Relaxed-preferred mAbs can inhibit FimH binding. (**A**) Inhibition of FimH$_{LD}$ binding to BSM at a 5:1 molar ratio of mAb to protein ($n \geq 3$). (**B**) Inhibition of UTI89 guinea pig erythrocyte hemagglutination ($n \geq 2$). Kp1 2H04 mAb inhibition of (**C**) Ec FimH$_{LD}$ and (**D**) Kp FimH$_{LD}$ binding to C3H/HeN mouse bladders. mAb was preincubated with FimH$_{LD}$ at a 10:1 molar ratio. Sections were stained with DNA dye Hoechst (blue), Ec or Kp FimH$_{LD}$ (red), and antibody to uroplakin III (green). $n = 4$ to 5 bladder sections with $n = 2$ technical replicates.

(hpi) (Fig. 5A). There was no detectable IgG in urine before infection (24 hours after intraperitoneal injection of mAbs), but mAbs were detected in the bladder ~3 to 6 hours after infection, consistent with bladder damage being necessary for antibodies to reach the urine as previously suggested (fig. S8) (*30*). Three of the mAbs from epitope Class 1 (Ec1 F7, Kp1 2H04, and Kp1 1A02), resulted in significantly decreased bladder titers (~1 log; $P < 0.05$) and two Class 1 mAbs (Ec1 F7 and Kp1 2H04) also significantly decreased kidney titers (~0.5 log; $P < 0.05$) (Fig. 5, B and C). The effect of prophylactic administration of Kp1 2H04, one of the strongest inhibitors of bladder titers at 24 hpi, on formation of intracellular bacterial communities (IBCs) at 6 hpi was assessed. Kp1 2H04 significantly decreased the amount of bladder IBCs compared to the control IgG at 6 hpi (Fig. 5, D to F).

To test whether immune system signaling functions associated with the fragment crystallizable (Fc) region of mAbs were needed for protection, we created a LALAPG Fc variant of Kp1 2H04 (2H04$_{LALAPG}$), which inhibits the ability of the mAb to bind Fc receptors or fix complement (*31*). 2H04$_{LALAPG}$ had a comparable binding affinity to FimH$_{LD}$ as 2H04 when assayed by ELISA (fig. S9). When tested in the prophylactic model, 2H04$_{LALAPG}$ inhibited UTI89 infection to the same degree as Kp1 2H04 in the bladder and kidney (Fig. 5, G and H), suggesting that Kp1 2H04 prevents infection primarily by directly inhibiting FimH rather than through Fc receptor functions. To further

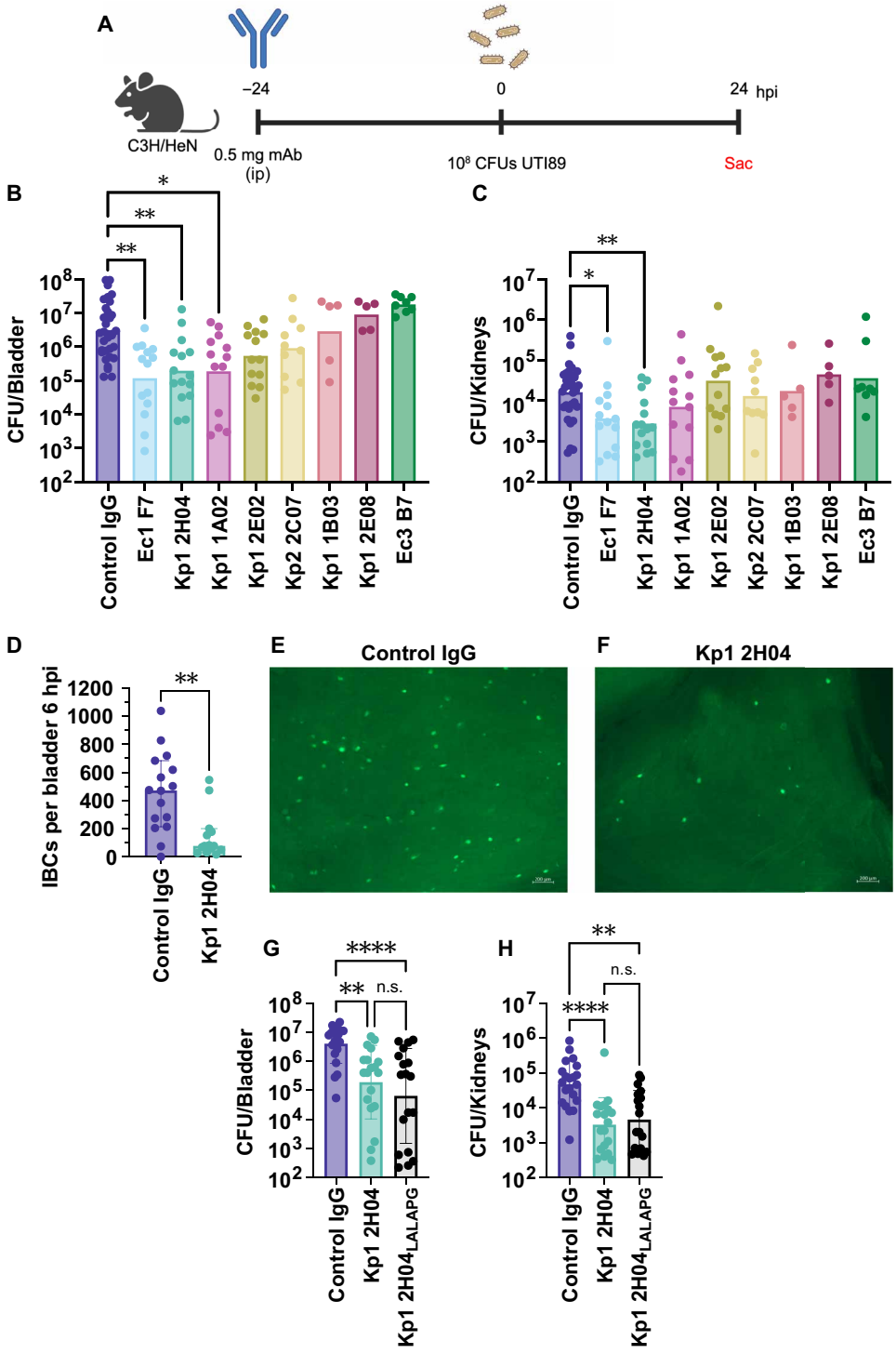

Fig. 5. FimH mAbs protect from *E. coli* UTI. (**A**) Six- to 7-week-old C3H/HeN mice were pretreated with 0.5 mg of mAb 24 hours before infection with UTI89. ip, intraperitoneal. (**B**) 24 hpi bladder and (**C**) kidney titers (for Kp1 1B03 and Kp1 2E08, $n = 5$ with one independent replicate; for Ec3 B7, $n = 8$ with one independent replicate; for Kp2 2C07, $n = 10$ with two independent replicates; and for control IgG, Ec1 F7, Kp1 2H04, Kp1 1A02, and Kp1 2E02, $n = 13$ to 33 with three independent replicates). (**D**) IBC counts at 6 hpi ($n = 16$ for control IgG; $n = 14$ for Kp1 2H04 with two independent replicates). Representative 5x magnification images of IBCs (green) in splayed mouse bladders for (**E**) control IgG and (**F**) Kp1 2H04 treatments. Scale bars, 200 μm. 24 hpi bladder (**G**) and kidney titers (**H**) from the prophylactic model testing control IgG, Kp1 2H04, and Kp1 2H04$_{LALAPG}$ ($n = 21$ for control group, $n = 20$ for Kp1 2H04, and $n = 19$ for Kp1 2H04$_{LALAPG}$ with three independent replicates). For (D), the bar graph represents the median with error bars of 95% confidence interval and a Mann-Whitney *U* test was used to evaluate statistical significance. For (B), (C), (G), and (H), bar graphs represent geometric means with error bars of SD and statistical comparisons were made using the Kruskal-Wallis test [nonparametric analysis of variance (ANOVA)] with Dunn's comparisons to the control group correcting for multiple comparisons. n.s., not significant; *$P \leq 0.05$; **$P \leq 0.01$; ****$P \leq 0.00001$. The schematic in (A) was created in BioRender. E.D.B.L. (2025), https://BioRender.com/a40t157.

test this, we repeated the prophylactic model but monitored the infection over 14 days. Kp1 2H04 treated mice resulted in lower urine and bladder titers over the 14 days. Still, this difference did not increase over time despite detectable amounts of mAb in the serum and bladder homogenates up to 14 days postinfection; however, this infection model may lack the resolution necessary to distinguish these titer differences as a portion of mice can naturally resolve infection in 2 weeks (fig. S10). These results suggest that the primary mechanism of the mAb is blocking initial FimH attachment to the bladder epithelium.

DISCUSSION

Carbapenem-resistant *Enterobacteriaceae* (CRE) and extended-spectrum beta-lactamase (ESBL) producing *Enterobacteriaceae* are listed as urgent and serious threats by the US Centers for Disease Control and Prevention (CDC) as they are resistant to numerous antibiotics needed to treat common infections, including UTIs (*32*, *33*). New antibiotic-sparing strategies are needed to treat these and other *Enterobacteriaceae* infections. mAbs have been exceptional drugs in treating cancer and viral infections (*34*–*38*), but few mAb therapies have been notably developed for treating or preventing bacterial infections. Here, we generated mAbs to neutralize FimH, the critical adhesin used by UPEC and *K. pneumoniae* to mediate UTI pathogenesis. We (i) generated mAbs that define four classes of anti-FimH mAbs that bind to distinct FimH epitopes, (ii) identified cross-reactive mAbs with high affinity to *E. coli* and *K. pneumoniae* FimH, and (iii) characterized the most potent FimH blocking antibodies in a structural and functional analysis. When we tested these mAbs in vivo, we found that significant quantities of antibody could be detected in the urine of mice after (but not prior to) infection, suggesting that mAbs penetrate the urinary tract in the context of infection. Two Class 1 Kp and Ec mAbs (Kp1 2H04 and Ec1 F7) significantly reduced bacterial titers in the bladder and kidneys when administered before UPEC infection in a robust mouse model of UTI through direct inhibition of FimH function. This is in contrast to previous studies suggesting that mAbs to the relaxed FimH conformation may stabilize a high-affinity conformation thereby increasing affinity to the bladder (*39*, *40*). These data suggest that some mAbs, which bind outside the binding pocket to a high-affinity relaxed conformation by our structural analysis, inhibit FimH binding through steric hindrance preventing access to the binding pocket.

FimH mAbs were tested in a prophylactic administration model to represent a probable clinical use of efficacious mAb administration. One population where prophylactic administration of FimH mAbs may be particularly advantageous is patients who are highly susceptible to UTIs, such as patients with a history of recurrent UTIs and catheterized patients. This represents a large patient population as between 20 and 30% of all women who get an initial UTI will suffer from a recurrent UTI and catheter-associated urinary tract infections account for up to 40% of all hospital-acquired infections (*41*–*44*). In the murine challenge model used in this study, the bladder was directly inoculated with a large amount of UPEC [10^8 colony-forming units (CFUs)] and preadministration of the mAbs resulted in an ~1.5 log (>95%) decrease in bladder colonization. In the context of patients, UTIs are likely seeded from much less bacteria, suggesting that protection from FimH mAbs in clinical populations may be more efficacious. Our results suggested that the mAbs inhibit FimH binding leading to protection as protection was Fc independent. After initial FimH-mediated attachment to the bladder epithelium, UPEC and *K. pneumoniae* invade the bladder cells and form persistent IBCs, which are difficult to treat (*45*). Although these communities can flux out of the cell and use FimH to invade neighboring cells, UPEC and *K. pneumoniae* use many other virulence factors involved in IBC formation and infection persistence (*27*, *46*–*48*). Thus, whereas FimH mAbs prevented IBC formation and were detectable in the bladder for 2 weeks, treatment of established UTI with FimH mAbs may prove more difficult.

In the bladder, FimH binds uroplakin Ia, which forms an oligomeric complex with other uroplakin proteins in a dense crystalline lipid superstructure burying the mannose glycan deep in the complex (*49*). The structure of uroplakin plaques requires FimH to reach into a tight spatial pocket to bind mannose. One speculative model for binding inhibition in the bladder is steric hindrance by the binding of mAbs preventing FimH from reaching the mannose on uroplakin (fig. S11). In addition, this steric hindrance model may apply to FimH binding of BSM and erythrocytes in our assays, which can be heavily glycosylated and, for BSM, are prone to dense aggregation; however, the atomic modeling of FimH binding to these substrates is less well known. This proposed mechanism does not preclude the additional possibility of stabilizing the high-affinity conformation as shifting the conformational equilibrium toward the high-affinity state via mutations can also result in virulence attenuation (*20*, *50*, *51*). Although we did not observe a shift to higher affinity in in vitro binding assays, we cannot rule out that allosteric effects on the FimH conformational equilibrium from the mAbs may contribute to protection. Bacteria with low-affinity tense-shifted FimH alleles may be able to evade vaccination or mAb therapy targeting the relaxed FimH conformation; however, bacteria with tense-shifted FimH alleles are attenuated in infection due to decreased ability to bind to the bladder epithelium (*21*, *50*, *51*). Nevertheless, the highly variable ability of antibodies to bind to tense or relaxed states of FimH suggests that the conformational equilibrium may provide an advantage in vivo by helping UPEC avoid antibodies that effectively bind to only one of the two states. Notably, we did not identify a mAb that directly binds to the FimH mannose-binding pocket, suggesting that vaccination of FimH in the relaxed state may function by providing antibodies that sterically inhibit FimH rather than directly blocking the mannose-binding pocket. Future studies are needed to determine the antigenicity of a tense state FimH and whether tense state–specific anti-FimH mAbs are effective at protecting from UTI.

Our results show that FimH-inhibiting mAbs have promising antibiotic-sparing therapeutic potential to treat both UPEC and *K. pneumoniae* UTIs, lay the groundwork for identifying FimH mAbs with increased efficacy, and provide a roadmap to leverage mAbs to inhibit other bacterial uropathogenic CUP adhesins. Although there have been few mAbs developed to treat bacterial infection, mAbs directed at treating UTI could offer unique advantages over antibiotics because they both avoid selection of antibiotic resistance and would have a sustained period of effectiveness. These mAbs may be deployed effectively in patients with highly recurrent UTI, who are often administered prophylactic antibiotics, or in hospital settings with patients with high-risk UTI, such as patient populations requiring catheterization, in which UPEC and *K. pneumoniae* can repeatedly colonize catheters over many months (*52*).

MATERIALS AND METHODS

Protein generation, purification, and bacterial strains

FimCH, $FimH_{LD}$, and FmlH lectin domain truncated proteins were purified as previously described (*21*, *27*, *50*, *53*). Bacterial strains used for this study, including those used in protein expression, are listed in table S2. Briefly, proteins were expressed and isolated from crude periplasmic preparations using affinity chromatography. In vitro donor strand exchange using the $FimG_{NTE}$ peptide was performed and purified as previously published (*20*). $FimH_{LD}$ labeled with the EZ-Link NHS-PEG4 Biotinylation Kit (Thermo Fisher Scientific, catalog no. A39259) or Alexa Fluor 647 with NHS Ester conjugation (Invitrogen, catalog no. A20006) was generated according to the manufacturer's instructions. Surface topology diagram of FimH was generated using PDBsum (*54*).

Mouse immunization for mAb generation

All procedures involving animals were performed in accordance with the guidelines of the Institutional Animal Care and Use Committee (IACUC) of Washington University in Saint Louis. Female 6- to 7-week-old C57BL/6J mice (the Jackson Laboratory, catalog no. 000664, RRID:IMSR_JAX:000664) were immunized intramuscularly with 30 μg of *E. coli* $FimH_{LD}$ or 25 μg of *K. pneumoniae* $FimH_{LD}$ emulsified with AddaVax (InvivoGen; catalog no. ac-adx-10). Four weeks later, mice were boosted with a second dose of $FimH_{LD}$ emulsified with AddaVax. One control mouse received phosphate-buffered saline (PBS) emulsified with AddaVax according to the same schedule. Draining iliac and inguinal lymph nodes were harvested 5 days after the boost for plasmablast sorting.

Cell sorting for mAb generation

Staining for sorting was performed using fresh lymph node single-cell suspensions in PBS supplemented with 2% fetal bovine serum (FBS) and 1 mM EDTA (P2). Cells were stained for 30 min on ice with CD138-BV421 (281-2, 1:200), CD4-PerCP (GK1.5, 1:100), CD19-PE (6D5, 1:200), B220-PE-D594 (RA3-6B2, 1:200), CD38-PE-Cy7 (90, 1:200), Fas-APC (SA367H8, 1:400), IgD-APC-Cy7 (11-26c.2a, 1:100), and Zombie Aqua (all BioLegend) diluted in P2. Cells were washed twice, and single plasmablasts (B220lo CD138+ IgDlo CD19+ CD4− live singlet lymphocytes) were sorted using a FACSAria II into 96-well plates containing 2 μl of lysis buffer (Clontech, catalog no. 420301) supplemented with RNase inhibitor (1 U/μl; NEB, catalog no. M0314L) and immediately frozen on dry ice.

mAb and Fab generation

Antibodies were cloned as previously described (*26*, *55*). In brief, VH, Vκ, and Vλ genes were amplified by reverse transcription polymerase chain reaction (RT-PCR) and nested PCR from singly sorted plasmablasts using cocktails of primers specific for IgG, IgM/A, Igκ, and Igλ using first-round and nested primer sets (*26*, *55*–*57*) (table S3) and then sequenced. Clonally related cells were identified by the same length and composition of IGHV, IGHJ, and heavy chain CDR3 and shared somatic hypermutation at the nucleotide level. To generate recombinant antibodies, heavy chain V-D-J and light chain V-J fragments were PCR amplified from first-round PCR products with mouse variable gene forward primers and joining gene reverse primers having 5′ extensions for cloning by Gibson assembly as previously described (*58*) (table S3) and were cloned into pABVec6W antibody expression vectors (*59*) in frame with either human IgG, IgK, or IgL constant domain. Sequences for variable heavy and light chain variable regions of these mAbs are listed in table S6. Plasmids were cotransfected at a 1:2 heavy chain–to–light chain ratio into Expi293F cells (RRID:CVCL_D615) using the Expifectamine 293 Expression Kit (Thermo Fisher Scientific; catalog no. A14525), and antibodies were purified with protein A agarose (Goldbio, catalog no. P-400-50). For monovalent Fab generation, the VH segment of selected antibodies was cloned into a Fab expression vector with a thrombin cleavage site preceding a 6xHis tag by GenScript. Fab and light chain plasmids were cotransfected into Expi293F cells for expression and purified with HisPur Ni-NTA resin (Thermo Fisher Scientific, catalog no. 88222). For controls in experiments, IgG mAb 2B04, specific for SARS-CoV-2 (severe acute respiratory syndrome coronavirus 2) receptor binding domain (*55*), was used.

Enzyme-linked immunosorbent assays

To generate ELISA binding curves to $FimH_{LD}$ and $FmlH_{LD}$ adhesin truncates, plates were first coated with the antigen (0.1 μg/ml) overnight. Plates were washed once with PBS supplemented with Tween 20 (PBS-T; 0.05%) and blocked for 2 hours with PBS-T with 10% FBS. mAbs were serially diluted starting at 30 μg/ml and added to the plate to bind for 1 hour. Plates were washed 3x in PBS-T. mAb binding was detected with anti-human IgG (Jackson ImmunoResearch, 1:2500 dilution, catalog no. 109-035-088, RRID:AB_233758) for 1 hour before washing three times in PBS-T and developed with *O*-phenylenediamine dihydrochloride in citrate buffer (Sigma-Aldrich). Reactions were quenched with 1 M HCl, and absorbance was read at 490 nm. Results reported are representative of three or more biological replicates.

To measure inhibition of $FimH_{LD}$ binding, plates were coated with BSM (10 μg/ml) overnight. Plates were blocked for 2 hours with 1x PBS with 1% bovine serum albumin (BSA). $FimH_{LD}$ (2.5 μg/ml) was mixed with a serial curve of mAb (to ensure dose-dependent inhibition) for 1 hour. $FimH_{LD}$ mAb mixtures were then added to the plate to let bind for 1 hour at room temperature. Plates were washed three times with PBS-T and incubated with anti-streptavidin–horseradish peroxidase (HRP) (BD Pharmagen, catalog no. 554066) for 1 hour before washing three times with PBS-T and development with 3,3′, 5,5′ tetramethylbenzidine (TMB) substrate (BD Pharmagen, catalog no. 555214). Reactions were quenched with 1 M H_2SO_4, and absorbance at 450 nm was recorded. Results reported are average of three or more biological replicates.

For measurements of the reactivity of mAbs to bacteria, bacteria were grown statically 2x24 (grown for 24 hours and subcultured 1:1000 for another 24 hours of growth period) in LB and normalized to OD_{600} (optical density at 600 nm) = 1.0 in 1x PBS. Bacteria (100 μl) were added to the plate, spun down for 5 min at 3000 rcf, and allowed to bind for 1 hour. The supernatant was decanted and formalin (10%) was added to the wells to fix bacteria for 10 min. Plates were washed 3x in PBS-T and then assayed and developed with the same protocol as the ELISA binding curves to adhesin truncates. Results reported are average of three or more biological replicates.

To measure levels of humanized IgG (mAbs) in serum, urines, and bladder homogenates, plates were coated with diluted 1:100 serum, 1:10 mouse urine, or 1:2 bladder homogenates along with a standard curve of hIgG isotype overnight at 4°C. Plates were then blocked for 2 hours at room temperature with 1x PBS with 1% BSA. Then, plates were washed three times with PBS-T. To measure hIgG levels, plates were then incubated with 1:10,000 dilution of goat anti-human IgG H&L (HRP) preabsorbed IgG (Abcam, catalog

no. ab97175, RRID:AB_10680841) for 1 hour at room temperature. For plate development, TMB substrate reagent was added and incubated for ~5 min at room temperature. Reactions were quenched with 3 M HCl, and absorbance at 450 nm was recorded. Results reported are average of three or more biological replicates.

Generation of FimH surface mutants

Surface FimH (J96) mutants were generated via one-step mutagenesis (*60*) using a pBAD33.1 vector plasmid encoding for FimH (J96 strain) template, Pfu Ultra HF polymerase (Agilent, catalog no. NC9666083), and the primers listed in table S5. After PCR amplification, reactions were digested with DpnI (NEB Biolabs, catalog no. R0176S) to remove the original template from the reaction products. PCR products were transformed into *E. coli* DH5α for ligation. Plasmids confirmed by Sanger sequencing were then transformed into the *E. coli* C600 Δ*fim* expression strain.

Epitope mapping

Epitope mapping of FimH mAbs to *E. coli* $FimC_{his}H$ was performed using a modified ELISA technique. The *E. coli* strain C600 Δ*fim*, carrying pBAD33 plasmids encoding FimH mutants and a ptrc99a plasmid encoding $FimC_{his}$, were grown in LB to an OD of 0.6 to 0.8 and then induced with 0.1 mM IPTG (isopropyl-β-D-thiogalactopyranoside) and 0.05% arabinose for 1 hour. Cells were harvested, and periplasm extracts containing $FimC_{his}H$ variants were obtained (*53*). $FimC_{his}H$ periplasmic extracts were titrated using anti-FimH sera to normalize the amount of FimH. Normalized $FimC_{his}H$ periplasm was used to coat plates for 1 hour at room temperature. Plates were blocked for 2 hours with 1x PBS with 1% BSA, and mAbs [0.1 μg/ml, except if low-binding mAb 2A02 (1 μg/ml) was used] were allowed to bind for 1 hour. Plates were washed in 1x PBS-T before detection with anti-human IgG (Jackson ImmunoResearch, 1:1000 dilution) and developed with TMB substrate (BD Pharmagen) and H_2SO_4 as outlined above. mAb binding to each $FimC_{his}H$ mutant was normalized to wild-type (WT) $FimC_{his}H$ binding. Variants that decreased binding below 17% of WT binding and clustered together on the structure of $FimH_{LD}$ (three or more residues) were considered an epitope. The 17% cutoff was chosen as this gave distinct structural cluster groupings and larger cutoffs resulted in more nonclustered mutant hits on the $FimH_{LD}$ structure. Epitope mapping was repeated three independent times. Mapping data were visualized and clustered (one-minus Pearson correlation) in Morpheus (https://software.broadinstitute.org/morpheus).

Western blotting

Western blotting to detect FimA in bacterial lysates was performed as previously published (*21*). Bacteria grown 2x24 statically was normalized to $OD_{600} = 1.0$ and were acid treated with HCl and boiled to disrupt FimA DSE interactions. To measure FimA, rabbit antitype 1 pili (1:2000) was used. A secondary antibody of goat anti-rabbit–HRP (1:10,000, KPL, catalog no. 5220-0336, RRID:AB_2857917) was used to detect followed by development with SuperSignal West Femto Maximum Sensitivity Substrate (Thermo Fisher Scientific, catalog no. 34579). Images were obtained on a Bio-Rad ChemiDoc system. A colorimetric image (to view the protein size ladder) was overlaid on the chemiluminescent image (detection signal) to mark the approximate size of the band in the figure reported in this study, which is representative of three independent biological replicates.

BLI studies

Kinetic binding studies were performed on an Octet Red instrument (ForteBio). Avi-tag biotinylated Fabs were loaded up to 2.5 nm onto Streptavidin sensor tips (Sartorius) that were preequilibrated in Hepes-buffered saline with 0.05% Tween 20 and 1% BSA (kinetic buffer A). Diluted antigens (Ec $FimH_{LD}$ and Ec $FimG_{nte}H$) were monitored for 200 s of association and 600 s of dissociation in kinetic buffer A. Loaded sensor tips dipping in kinetic buffer A were used as reference sensors. Reference-subtracted kinetic traces were used to calculate kinetic rate constants (k_{on} and k_{off}) and equilibrium dissociation rate constant (K_D) using a Langmuir 1:1 binding model. Resulting binding traces and fits were plotted with GraphPad Prism v10.

Hemagglutination inhibition assay

E. coli guinea pig erythrocyte hemagglutination inhibition assays were performed as previously described (*61*). Briefly, mAbs were serially diluted in microtiter plates, and 25 μl of bacterial suspension (serially diluted from $OD_{600} = 10.0$ in 1x PBS) was added to each well. After incubation for 10 min at room temperature, 25 μl ($OD_{640} = 2.0$) of guinea pig erythrocytes in 1x PBS was added for a final volume of 50 μl. The plates were incubated at 4°C overnight. For each mAb concentration, the hemagglutinin (HA) titer was defined as the greatest dilution of bacteria that caused hemagglutination.

Cryo-EM data collection and analysis

Fab and FimCH protein were mixed at a ratio of 1.2:1 and dialyzed into 20 mM Hepes (pH 7.5) with 50 mM NaCl. Complexes were flash frozen on EM grids in liquid ethane using an FEI Vitrobot (Thermo Fisher Scientific) and imaged on Titan Krios (2H04 complex) or Glacios (F7, B7, and 2C07 complexes) microscopes using a Falcon 4 electron detector (Thermo Fisher Scientific). Movies were processed in Cryosparc v4.4.1 (*62*, *63*), and particles were picked using Topaz (*64*). Densities were postprocessed using DeepEMhancer (*64*) for model building. The collection parameters and workflow are described in more detail in fig. S3. Initial Fab models were built using homology models in SwissModel (*65*). The $FimH_{LD}$ model was generated by trimming and threading the UTI89 FimH sequence on Protein Data Bank (PDB) 1KLF. Rough models were initially docked in ChimeraX (*66*) before multiple rounds of real-space refinement in Phenix v1.20.1 (*67*) with manual editing in COOT v0.9.6 (*68*). Refinement statistics are shown in table S4.

Immunofluorescence studies

Seven- to 8-week-old female C3H/HeN mice (Envigo) bladders were fixed in formalin, embedded in paraffin, and sectioned. Tissue sections were heat deparaffinized and rehydrated in xylene, followed by stepwise hydration in 100% ethanol, 90% ethanol, 75% ethanol, and 50% ethanol to 30% ethanol (each step having a 5-min incubation in fresh solution). Slides were rinsed in 1x PBS followed by blocking solution (1x PBS with 5% FBS). Primary mouse antibody to uroplakin IIIa (Thermo Fisher Scientific, 1:50, catalog no. 690108S, RRID:AB_2904126) was allowed to bind overnight at 4°C. Slides were washed in 1x PBS, and a secondary anti-mouse Alexa Fluor 488 antibody (Invitrogen, 1:1000, catalog no. A21202, RRID:AB_141607) was allowed to bind for 2 hours and then washed again. $FimH_{LD}$–Alexa Fluor 647 (588 nM) was mixed with mAb (6 μM) for 20 min at room temperature in 1x PBS. $FimH_{LD}$ mAb mixtures were applied to the section along with Hoechst DNA dye (8 μM) for 20 min at room

temperature. The slides were washed again in 1x PBS and allowed to dry. ProLong Gold Antifade Mountant (Invitrogen, catalog no. P36930) was added, and slides were imaged using the confocal function of a Zeiss Cell Observer Spinning Disk Confocal Microscope with a 10x air objective lens.

Splayed bladders were analyzed with a Zeiss Axio Observer D1 inverted fluorescence microscope equipped with an X-Cite120 mini LED light source (Excelitis Technologies) and 4′,6-diamidino-2-phenylindole (DAPI), green fluorescent protein (GFP), DsRed, and Cy5 filter sets. EC Plan-Neofluar [numerical aperture (NA) 0.075] 2.5X and EC Plan-Neofluar (NA 0.15) 5X objectives (Zeiss), an Axiocam 503 color camera (Zeiss), and ZEN 2 (blue version) software were used for image acquisition.

Mouse infection experiments

For acute and 2-week infection models, 7- to 8-week-old female C3H/HeN mice (Envigo, catalog no. 040, RRID:IMSR_ENV:HSD-040) were infected with 2×10^8 CFUs of UTI89 as previously described (*69*). Intraperitoneal injections of mAb were given in 1x PBS buffer 24 hours before infection. Urines were taken by clean catch at specified time points. For obtaining serum, three to four mice per treatment group were bled at specific time points during the length of the experiment via a submental bleeding method. At the conclusion of the experimental time points, mice were humanely euthanized and bladder and kidney organs were homogenized and tittered. For screening mAbs in the prophylactic infection model with UTI89, if a phenotype was observed after one replicate, the experiment was repeated an additional one to two times. Sample sizes were informed from previous mouse studies (*70*, *71*). All studies were approved and performed in accordance with the guidelines set by the Committee for Animal Studies at Washington University School of Medicine under IACUC protocols 21-0341 and 21-0394 (IACUC Protocol Approval Animal Welfare Assurance no. D16-00245).

Supplementary Materials

This PDF file includes:

Figs. S1 to S11
Tables S1 to S6
References

REFERENCES AND NOTES

1. X. Yang, H. Chen, Y. Zheng, S. Qu, H. Wang, F. Yi, Disease burden and long-term trends of urinary tract infections: A worldwide report. *Front. Public Health* **10**, 888205 (2022).
2. Z. Zeng, J. Zhan, K. Zhang, H. Chen, S. Cheng, Global, regional, and national burden of urinary tract infections from 1990 to 2019: An analysis of the global burden of disease study 2019. *World J. Urol.* **40**, 755–763 (2022).
3. J. E. Simmering, F. Tang, J. E. Cavanaugh, L. A. Polgreen, P. M. Polgreen, The increase in hospitalizations for urinary tract infections and the associated costs in the United States, 1998–2011. *Open Forum Infect. Dis.* **4**, ofw281 (2017).
4. D. Scholes, T. M. Hooton, P. L. Roberts, A. E. Stapleton, K. Gupta, W. E. Stamm, Risk factors for recurrent urinary tract infection in young women. *J. Infect. Dis.* **182**, 1177–1182 (2000).
5. C. W. Seymour, F. Gesten, H. C. Prescott, M. E. Friedrich, T. J. Iwashyna, G. S. Phillips, S. Lemeshow, T. Osborn, K. M. Terry, M. M. Levy, Time to treatment and mortality during mandated emergency care for sepsis. *N. Engl. J. Med.* **376**, 2235–2244 (2017).
6. J. Hrbacek, P. Cermak, R. Zachoval, Current antibiotic resistance trends of uropathogens in Central Europe: Survey from a tertiary hospital urology department 2011-2019. *Antibiotics (Basel)* **9**, 630 (2020).
7. B. Kot, Antibiotic resistance among uropathogenic *Escherichia coli*. *Pol. J. Microbiol.* **68**, 403–415 (2019).
8. S. Navon-Venezia, K. Kondratyeva, A. Carattoli, *Klebsiella pneumoniae*: A major worldwide source and shuttle for antibiotic resistance. *FEMS Microbiol. Rev.* **41**, 252–275 (2017).
9. A. L. Flores-Mireles, J. N. Walker, M. Caparon, S. J. Hultgren, Urinary tract infections: Epidemiology, mechanisms of infection and treatment options. *Nat. Rev. Microbiol.* **13**, 269–284 (2015).
10. Antimicrobial Resistance Collaborators, Global burden of bacterial antimicrobial resistance in 2019: A systematic analysis. *Lancet* **399**, 629–655 (2022).
11. J. J. Martinez, M. A. Mulvey, J. D. Schilling, J. S. Pinkner, S. J. Hultgren, Type 1 pilus-mediated bacterial invasion of bladder epithelial cells. *EMBO J.* **19**, 2803–2812 (2000).
12. D. A. Rosen, J. S. Pinkner, J. N. Walker, J. S. Elam, J. M. Jones, S. J. Hultgren, Molecular variations in *Klebsiella pneumoniae* and *Escherichia coli* FimH affect function and pathogenesis in the urinary tract. *Infect. Immun.* **76**, 3346–3356 (2008).
13. L. K. McLellan, M. R. McAllaster, A. S. Kim, Ľ. Tóthová, P. D. Olson, J. S. Pinkner, A. L. Daugherty, T. N. Hreha, J. W. Janetka, D. H. Fremont, S. J. Hultgren, H. W. Virgin, D. A. Hunstad, A host receptor enables type 1 pilus-mediated pathogenesis of *Escherichia coli* pyelonephritis. *PLOS Pathog.* **17**, e1009314 (2021).
14. M. A. Mulvey, J. D. Schilling, S. J. Hultgren, Establishment of a persistent *Escherichia coli* reservoir during the acute phase of a bladder infection. *Infect. Immun.* **69**, 4572–4579 (2001).
15. D. A. Rosen, J. S. Pinkner, J. M. Jones, J. N. Walker, S. Clegg, S. J. Hultgren, Utilization of an intracellular bacterial community pathway in *Klebsiella pneumoniae* urinary tract infection and the effects of FimK on type 1 pilus expression. *Infect. Immun.* **76**, 3337–3345 (2008).
16. G. G. Anderson, J. J. Palermo, J. D. Schilling, R. Roth, J. Heuser, S. J. Hultgren, Intracellular bacterial biofilm-like pods in urinary tract infections. *Science* **301**, 105–107 (2003).
17. V. P. O'Brien, T. J. Hannan, L. Yu, J. Livny, E. D. O. Roberson, D. J. Schwartz, S. Souza, C. L. Mendelsohn, M. Colonna, A. L. Lewis, S. J. Hultgren, A mucosal imprint left by prior Escherichia coli bladder infection sensitizes to recurrent disease. *Nat. Microbiol.* **2**, 16196 (2017).
18. S. K. Russell, J. K. Harrison, B. S. Olson, H. J. Lee, V. P. O'Brien, X. Xing, J. Livny, L. Yu, E. D. O. Roberson, R. Bomjan, C. Fan, M. Sha, S. Estfanous, A. O. Amer, M. Colonna, T. S. Stappenbeck, T. Wang, T. J. Hannan, S. J. Hultgren, Uropathogenic *Escherichia coli* infection-induced epithelial trained immunity impacts urinary tract disease outcome. *Nat. Microbiol.* **8**, 875–888 (2023).
19. D. Choudhury, A. Thompson, V. Stojanoff, S. Langermann, J. Pinkner, S. J. Hultgren, S. D. Knight, X-ray structure of the FimC-FimH chaperone-adhesin complex from uropathogenic *Escherichia coli*. *Science* **285**, 1061–1066 (1999).
20. V. Kalas, J. S. Pinkner, T. J. Hannan, M. E. Hibbing, K. W. Dodson, A. S. Holehouse, H. Zhang, N. H. Tolia, M. L. Gross, R. V. Pappu, J. Janetka, S. J. Hultgren, Evolutionary fine-tuning of conformational ensembles in FimH during host-pathogen interactions. *Sci. Adv.* **3**, e1601944 (2017).
21. E. D. B. Lopatto, J. S. Pinkner, D. A. Sanick, R. F. Potter, L. X. Liu, J. Bazán Villicaña, K. O. Tamadonfar, Y. Ye, M. I. Zimmerman, N. C. Gualberto, K. W. Dodson, J. W. Janetka, D. A. Hunstad, S. J. Hultgren, Conformational ensembles in *Klebsiella pneumoniae* FimH impact uropathogenesis. *Proc. Natl. Acad. Sci. U.S.A.* **121**, e2409655121 (2024).
22. G. R. Eldridge, H. Hughey, L. Rosenberger, S. M. Martin, A. M. Shapiro, E. D'Antonio, K. G. Krejci, N. Shore, J. Peterson, A. S. Lukes, C. M. Starks, Safety and immunogenicity of an adjuvanted *Escherichia coli* adhesin vaccine in healthy women with and without histories of recurrent urinary tract infections: Results from a first-in-human phase 1 study. *Hum. Vaccin. Immunother.* **17**, 1262–1270 (2021).
23. E. Perer, H. Stacey, T. Eichorn, H. Hughey, J. Lawrence, E. Cunningham, M. O. Johnson, K. Bacon, A. Kau, S. J. Hultgren, T. M. Hooton, J. L. Harris, Case report: Long-term follow-up of patients who received a FimCH vaccine for prevention of recurrent urinary tract infections caused by antibiotic resistant Enterobacteriaceae: A case report series. *Front. Immunol.* **15**, 1359738 (2024).
24. S. Langermann, S. Palaszynski, M. Barnhart, G. Auguste, J. S. Pinkner, J. Burlein, P. Barren, S. Koenig, S. Leath, C. H. Jones, S. J. Hultgren, Prevention of mucosal *Escherichia coli* infection by FimH-adhesin-based systemic vaccination. *Science* **276**, 607–611 (1997).
25. S. Langermann, R. Möllby, J. E. Burlein, S. R. Palaszynski, C. G. Auguste, A. DeFusco, R. Strouse, M. A. Schenerman, S. J. Hultgren, J. S. Pinkner, J. Winberg, L. Guldevall, M. Söderhäll, K. Ishikawa, S. Normark, S. Koenig, Vaccination with FimH adhesin protects cynomolgus monkeys from colonization and infection by uropathogenic *Escherichia coli*. *J. Infect. Dis.* **181**, 774–778 (2000).
26. L. Von Boehmer, C. Liu, S. Ackerman, A. D. Gitlin, Q. Wang, A. Gazumyan, M. C. Nussenzweig, Sequencing and cloning of antigen-specific antibodies from mouse memory B cells. *Nat. Protoc.* **11**, 1908–1923 (2016).
27. M. S. Conover, S. Ruer, J. Taganna, V. Kalas, H. De Greve, J. S. Pinkner, K. W. Dodson, H. Remaut, S. J. Hultgren, Inflammation-induced adhesin-receptor interaction provides a fitness advantage to uropathogenic *E. coli* during chronic infection. *Cell Host Microbe* **20**, 482–492 (2016).
28. D. I. Kisiela, P. Magala, G. Interlandi, L. A. Carlucci, A. Ramos, V. Tchesnokova, B. Basanta, V. Yarov-Yarovoy, H. Avagyan, A. Hovhannisyan, W. E. Thomas, R. E. Stenkamp, R. E. Klevit,

E. V. Sokurenko, Toggle switch residues control allosteric transitions in bacterial adhesins by participating in a concerted repacking of the protein core. *PLOS Pathog.* **17**, e1009440 (2021).
29. I. Le Trong, P. Aprikian, B. A. Kidd, M. Forero-Shelton, V. Tchesnokova, P. Rajagopal, V. Rodriguez, G. Interlandi, R. Klevit, V. Vogel, R. E. Stenkamp, E. V. Sokurenko, W. E. Thomas, Structural basis for mechanical force regulation of the adhesin FimH via finger trap-like β sheet twisting. *Cell* **141**, 645–655 (2010).
30. A. L. Flores-Mireles, J. N. Walker, A. Potretzke, H. L. Schreiber IV, J. S. Pinkner, T. M. Bauman, A. M. Park, A. Desai, S. J. Hultgren, M. G. Caparon, Antibody-based therapy for enterococcal catheter-associated urinary tract infections. *mBio* **7**, e01653-16 (2016).
31. T. Schlothauer, S. Herter, C. F. Koller, S. Grau-Richards, V. Steinhart, C. Spick, M. Kubbies, C. Klein, P. Umaña, E. Mössner, Novel human IgG1 and IgG4 Fc-engineered antibodies with completely abolished immune effector functions. *Protein Eng. Des. Sel.* **29**, 457–466 (2016).
32. CDC, 2019 Antibiotic Resistance Threats Report, https://cdc.gov/antimicrobial-resistance/data-research/threats/index.html.
33. CDC, Antimicrobial Resistance Threats in the United States, 2021–2022, https://cdc.gov/antimicrobial-resistance/data-research/threats/update-2022.html.
34. C. H. Chau, P. S. Steeg, W. D. Figg, Antibody–drug conjugates for cancer. *Lancet* **394**, 793–804 (2019).
35. D. Corti, L. A. Purcell, G. Snell, D. Veesler, Tackling COVID-19 with neutralizing monoclonal antibodies. *Cell* **184**, 3086–3108 (2021).
36. M. P. Griffin, Y. Yuan, T. Takas, J. B. Domachowske, S. A. Madhi, P. Manzoni, E. A. F. Simões, M. T. Esser, A. A. Khan, F. Dubovsky, T. Villafana, J. P. DeVincenzo, Nirsevimab Study Group, Single-dose nirsevimab for prevention of RSV in preterm infants. *N. Engl. J. Med.* **383**, 415–425 (2020).
37. S. Mulangu, L. E. Dodd, R. T. Davey Jr., O. T. Mbaya, M. Proschan, D. Mukadi, M. L. Manzo, D. Nzolo, A. T. Oloma, A. Ibanda, R. Ali, S. Coulibaly, A. C. Levine, R. Grais, J. Diaz, H. C. Lane, J.-J. Muyembe-Tamfum, PALM Writing Group, B. Sivahera, M. Camara, R. Kojan, R. Walker, B. Dighero-Kemp, H. Cao, P. Mukumbayi, P. Mbala-Kingebeni, S. Ahuka, S. Albert, T. Bonnett, I. Crozier, M. Duvenhage, C. Proffitt, M. Teitelbaum, T. Moench, J. Aboulhab, K. Barrett, K. Cahill, K. Cone, R. Eckes, L. Hensley, B. Herpin, E. Higgs, J. Ledgerwood, J. Pierson, M. Smolskis, Y. Sow, J. Tierney, S. Sivapalasingam, W. Holman, N. Gettinger, D. Vallée, J. Nordwall, PALM Consortium Study Team, A randomized, controlled trial of ebola virus disease therapeutics. *N. Engl. J. Med.* **381**, 2293–2303 (2019).
38. J. J. Lim, A. C. Nilsson, M. Silverman, N. Assy, P. Kulkarni, J. M. McBride, R. Deng, C. Li, X. Yang, A. Nguyen, P. Horn, M. Maia, A. Castro, M. C. Peck, J. Galanter, T. Chu, E. M. Newton, J. A. Tavel, A phase 2 randomized, double-blind, placebo-controlled trial of MHAA4549A, a monoclonal antibody, plus oseltamivir in patients hospitalized with severe influenza A virus infection. *Antimicrob. Agents Chemother.* **64**, e00352-20 (2020).
39. V. Tchesnokova, P. Aprikian, O. Yakovenko, C. LaRock, B. Kidd, V. Vogel, W. Thomas, E. Sokurenko, Integrin-like allosteric properties of the catch bond-forming FimH adhesin of *Escherichia coli*. *J. Biol. Chem.* **283**, 7823–7833 (2008).
40. V. Tchesnokova, P. Aprikian, D. Kisiela, S. Gowey, N. Korotkova, W. Thomas, E. Sokurenko, Type 1 fimbrial adhesin FimH elicits an immune response that enhances cell adhesion of *Escherichia coli*. *Infect. Immun.* **79**, 3895–3904 (2011).
41. B. Foxman, Epidemiology of urinary tract infections: Incidence, morbidity, and economic costs. *Dis. Mon.* **49**, 53–70 (2003).
42. R. C. L. Feneley, I. B. Hopley, P. N. T. Wells, Urinary catheters: History, current status, adverse events and research agenda. *J. Med. Eng. Technol.* **39**, 459–470 (2015).
43. T. M. Hooton, S. F. Bradley, D. D. Cardenas, R. Colgan, S. E. Geerlings, J. C. Rice, S. Saint, A. J. Schaeffer, P. A. Tambayh, P. Tenke, L. E. Nicolle, Infectious Diseases Society of America, Diagnosis, prevention, and treatment of catheter-associated urinary tract infection in adults: 2009 International Clinical Practice Guidelines from the Infectious Diseases Society of America. *Clin. Infect. Dis.* **50**, 625–663 (2010).
44. B. Foxman, Urinary tract infection syndromes: Occurrence, recurrence, bacteriology, risk factors, and disease burden. *Infect. Dis. Clin. North Am.* **28**, 1–13 (2014).
45. G. G. Anderson, S. M. Martin, S. J. Hultgren, Host subversion by formation of intracellular bacterial communities in the urinary tract. *Microbes Infect.* **6**, 1094–1101 (2004).
46. M. Hadjifrangiskou, A. P. Gu, J. S. Pinkner, M. Kostakioti, E. W. Zhang, S. E. Greene, S. J. Hultgren, Transposon mutagenesis identifies uropathogenic *Escherichia coli* biofilm factors. *J. Bacteriol.* **194**, 6195–6205 (2012).
47. M. S. Conover, M. Hadjifrangiskou, J. J. Palermo, M. E. Hibbing, K. W. Dodson, S. J. Hultgren, Metabolic requirements of *Escherichia coli* in intracellular bacterial communities during urinary tract infection pathogenesis. *mBio* **7**, e00104–e00116 (2016).
48. C. S. Reigstad, S. J. Hultgren, J. I. Gordon, Functional genomic studies of uropathogenic *Escherichia coli* and host urothelial cells when intracellular bacterial communities are assembled. *J. Biol. Chem.* **282**, 21259–21267 (2007).
49. H. Yanagisawa, Y. Kita, T. Oda, M. Kikkawa, Cryo-EM elucidates the uroplakin complex structure within liquid-crystalline lipids in the porcine urothelial membrane. *Commun. Biol.* **6**, 1018 (2023).
50. D. J. Schwartz, V. Kalas, J. S. Pinkner, S. L. Chen, C. N. Spaulding, K. W. Dodson, S. J. Hultgren, Positively selected FimH residues enhance virulence during urinary tract infection by altering FimH conformation. *Proc. Natl. Acad. Sci. U.S.A.* **110**, 15530–15537 (2013).
51. S. L. Chen, C. S. Hung, J. S. Pinkner, J. N. Walker, C. K. Cusumano, Z. Li, J. Bouckaert, J. I. Gordon, S. J. Hultgren, Positive selection identifies an in vivo role for FimH during urinary tract infection in addition to mannose binding. *Proc. Natl. Acad. Sci. U.S.A.* **106**, 22439–22444 (2009).
52. T. M. Nye, Z. Zou, C. L. P. Obernuefemann, J. S. Pinkner, E. Lowry, K. Kleinschmidt, K. Bergeron, A. Klim, K. W. Dodson, A. L. Flores-Mireles, J. N. Walker, D. G. Wong, A. Desai, M. G. Caparon, S. J. Hultgren, Microbial co-occurrences on catheters from long-term catheterized patients. *Nat. Commun.* **15**, 61 (2024).
53. J. Bouckaert, J. Berglund, M. Schembri, E. De Genst, L. Cools, M. Wuhrer, C. S. Hung, J. Pinkner, R. Slättegård, A. Zavialov, D. Choudhury, S. Langermann, S. J. Hultgren, L. Wyns, P. Klemm, S. Oscarson, S. D. Knight, H. De Greve, Receptor binding studies disclose a novel class of high-affinity inhibitors of the *Escherichia coli* FimH adhesin. *Mol. Microbiol.* **55**, 441–455 (2005).
54. R. A. Laskowski, Enhancing the functional annotation of PDB structures in PDBsum using key figures extracted from the literature. *Bioinformatics* **23**, 1824–1827 (2007).
55. W. B. Alsoussi, J. S. Turner, J. B. Case, H. Zhao, A. J. Schmitz, J. Q. Zhou, R. E. Chen, T. Lei, A. A. Rizk, K. M. McIntire, E. S. Winkler, J. M. Fox, N. M. Kafai, L. B. Thackray, A. O. Hassan, F. Amanat, F. Krammer, C. T. Watson, S. H. Kleinstein, D. H. Fremont, M. S. Diamond, A. H. Ellebedy, A Potently neutralizing antibody protects mice against SARS-CoV-2 infection. *J. Immunol.* **205**, 915–922 (2020).
56. T. Tiller, C. E. Busse, H. Wardemann, Cloning and expression of murine Ig genes from single B cells. *J. Immunol. Methods* **350**, 183–193 (2009).
57. M. Ehlers, H. Fukuyama, T. L. McGaha, A. Aderem, J. V. Ravetch, TLR9/MyD88 signaling is required for class switching to pathogenic IgG2a and 2b autoantibodies in SLE. *J. Exp. Med.* **203**, 553–561 (2006).
58. I. Y. Ho, J. J. Bunker, S. A. Erickson, K. E. Neu, M. Huang, M. Cortese, B. Pulendran, P. C. Wilson, Refined protocol for generating monoclonal antibodies from single human and murine B cells. *J. Immunol. Methods* **438**, 67–70 (2016).
59. C. W. Davis, K. J. L. Jackson, A. K. McElroy, P. Halfmann, J. Huang, C. Chennareddy, A. E. Piper, Y. Leung, C. G. Albariño, I. Crozier, A. H. Ellebedy, J. Sidney, A. Sette, T. Yu, S. C. A. Nielsen, A. J. Goff, C. F. Spiropoulou, E. O. Saphire, G. Cavet, Y. Kawaoka, A. K. Mehta, P. J. Glass, S. D. Boyd, R. Ahmed, Longitudinal analysis of the human B cell response to ebola virus infection. *Cell* **177**, 1566–1582.e17 (2019).
60. L. Zheng, U. Baumann, J.-L. Reymond, An efficient one-step site-directed and site-saturation mutagenesis protocol. *Nucleic Acids Res.* **32**, e115 (2004).
61. S. J. Hultgren, W. R. Schwan, A. J. Schaeffer, J. L. Duncan, Regulation of production of type 1 pili among urinary tract isolates of *Escherichia coli*. *Infect. Immun.* **54**, 613–620 (1986).
62. A. Punjani, J. L. Rubinstein, D. J. Fleet, M. A. Brubaker, cryoSPARC: Algorithms for rapid unsupervised cryo-EM structure determination. *Nat. Methods* **14**, 290–296 (2017).
63. A. Punjani, H. Zhang, D. J. Fleet, Non-uniform refinement: Adaptive regularization improves single-particle cryo-EM reconstruction. *Nat. Methods* **17**, 1214–1221 (2020).
64. T. Bepler, A. Morin, M. Rapp, J. Brasch, L. Shapiro, A. J. Noble, B. Berger, Positive-unlabeled convolutional neural networks for particle picking in cryo-electron micrographs. *Nat. Methods* **16**, 1153–1160 (2019).
65. A. Waterhouse, M. Bertoni, S. Bienert, G. Studer, G. Tauriello, R. Gumienny, F. T. Heer, T. A. P. De Beer, C. Rempfer, L. Bordoli, R. Lepore, T. Schwede, SWISS-MODEL: Homology modelling of protein structures and complexes. *Nucleic Acids Res.* **46**, W296–W303 (2018).
66. E. F. Pettersen, T. D. Goddard, C. C. Huang, E. C. Meng, G. S. Couch, T. I. Croll, J. H. Morris, T. E. Ferrin, UCSF ChimeraX: Structure visualization for researchers, educators, and developers. *Protein Sci.* **30**, 70–82 (2021).
67. D. Liebschner, P. V. Afonine, M. L. Baker, G. Bunkóczi, V. B. Chen, T. I. Croll, B. Hintze, L. W. Hung, S. Jain, A. J. McCoy, N. W. Moriarty, R. D. Oeffner, B. K. Poon, M. G. Prisant, R. J. Read, J. S. Richardson, D. C. Richardson, M. D. Sammito, O. V. Sobolev, D. H. Stockwell, T. C. Terwilliger, A. G. Urzhumtsev, L. L. Videau, C. J. Williams, P. D. Adams, Macromolecular structure determination using X-rays, neutrons and electrons: Recent developments in Phenix. *Acta Crystallogr. D Struct. Biol.* **75**, 861–877 (2019).
68. P. Emsley, B. Lohkamp, W. G. Scott, K. Cowtan, Features and development of Coot. *Acta Crystallogr. D Biol. Crystallogr.* **66**, 486–501 (2010).
69. T. J. Hannan, D. A. Hunstad, A murine model for *Escherichia coli* urinary tract infection. *Methods Mol. Biol.* **1333**, 159–175 (2016).
70. T. J. Hannan, I. U. Mysorekar, C. S. Hung, M. L. Isaacson-Schmid, S. J. Hultgren, Early severe inflammatory responses to uropathogenic *E. coli* predispose to chronic and recurrent urinary tract infection. *PLOS Pathog.* **6**, e1001042 (2010).
71. D. J. Schwartz, M. S. Conover, T. J. Hannan, S. J. Hultgren, Uropathogenic *Escherichia coli* superinfection enhances the severity of mouse bladder infection. *PLOS Pathog.* **11**, e1004599 (2015).

72. B. Xie, G. Zhou, S.-Y. Chan, E. Shapiro, X.-P. Kong, X.-R. Wu, T.-T. Sun, C. E. Costello, Distinct glycan structures of uroplakins Ia and Ib: Structural basis for the selective binding of FimH adhesin to uroplakin Ia. *J. Biol. Chem.* **281**, 14644–14653 (2006).
73. K. A. Datsenko, B. L. Wanner, One-step inactivation of chromosomal genes in *Escherichia coli* K-12 using PCR products. *Proc. Natl. Acad. Sci. U.S.A.* **97**, 6640–6645 (2000).
74. S. E. Greene, M. E. Hibbing, J. Janetk, S. L. Chen, S. J. Hultgren, Human urine decreases function and expression of type 1 pili in uropathogenic *Escherichia coli*. *mBio* **6**, e00820 (2015).
75. M. Kostakioti, M. Hadjifrangiskou, C. K. Cusumano, T. J. Hannan, J. W. Janetka, S. J. Hultgren, Distinguishing the contribution of type 1 pili from that of other QseB-misregulated factors when QseC is absent during urinary tract infection. *Infect. Immun.* **80**, 2826–2834 (2012).
76. K. J. Wright, P. C. Seed, S. J. Hultgren, Uropathogenic *Escherichia coli* flagella aid in efficient urinary tract colonization. *Infect. Immun.* **73**, 7657–7668 (2005).
77. I. U. Mysorekar, S. J. Hultgren, Mechanisms of uropathogenic *Escherichia coli* persistence and eradication from the urinary tract. *Proc. Natl. Acad. Sci. U.S.A.* **103**, 14170–14175 (2006).
78. I. Y. Ho, J. J. Bunker, S. A. Erickson, K. E. Neu, M. Huang, M. Cortese, B. Pulendran, P. C. Wilson, Refined protocol for generating monoclonal antibodies from single human and murine B cells. *J. Immunol. Methods* **438**, 67–70 (2016).

Acknowledgments: We thank A. Coyne, K. Tamadonfar, L. Liu, M. Zimmerman, N. Abdalla, T. Lei, and W. Beatty for assistance during this study. The mouse timeline graphics in Fig. 5A were created using BioRender. E.D.B.L. (2025), https://BioRender.com/a40t157. Cryo-EM and data collection were performed in part through the use of the Washington University Center for Cellular Imaging (WUCCI). **Funding:** This work was supported by the National Institutes of Health grants R01AI029549 (S.J.H.), R37AI048689 (S.J.H.), U19AI157797 (S.J.H. and A.H.E.), R01AI165915 (A.L.K.), and T32GM007067 (J.M.S.-B.) and Doris Duke Charitable Foundation 2019083 (A.L.K.). Cryo-EM was performed in part through the use of the Washington University Center for Cellular Imaging (WUCCI) supported by the Washington University School of Medicine, The Children's Discovery Institute of Washington University, and St. Louis Children's Hospital (CDI-CORE-2015-505 and CDI-CORE-2019-813) and the Foundation for Barnes-Jewish Hospital (3770 and 4642). **Author contributions:** Conceptualization: E.D.B.L., J.M.S.-B., K.W.D., A.H.E., A.L.K., and S.J.H. Methodology: E.D.B.L., J.M.S.-B., D.A.S., S.K.M., P.N.A., M.R.T., I.F.F., A.J.S., J.S.T., S.M.S., L.O., N.C.G., J.S.P., K.W.D., A.H.E., A.L.K., and S.J.H. Investigation: E.D.B.L., J.M.S.-B., D.A.S., S.K.M., P.N.A., M.R.T., I.F.F., A.J.S., J.S.T., S.M.S., L.O., N.C.G., J.S.P., K.W.D., A.H.E., A.L.K., and S.J.H. Visualization: E.D.B.L., J.M.S.-B., D.A.S., S.K.M., K.W.D., A.H.E., A.L.K., and S.J.H. Supervision: E.D.B.L., J.M.S.-B., K.W.D., A.H.E., A.L.K., and S.J.H. Writing—original draft: E.D.B.L., J.M.S.-B., K.W.D., A.H.E., A.L.K., and S.J.H. Writing—review and editing: E.D.B.L., J.M.S.-B., D.A.S., S.K.M., P.N.A., M.R.T., I.F.F., A.J.S., J.S.T., S.M.S., L.O., N.C.G., J.S.P., K.W.D., A.H.E., A.L.K., and S.J.H. **Competing interests:** Washington University in St. Louis has filed a nonprovisional US application (application number 19/097,433, FimH inhibiting compositions and methods of use thereof) on 1 April 2025 where the following authors on the present manuscript are listed as inventors: E.D.B.L., J.M.S.-B., D.A.S., M.R.T., I.F.F., A.J.S., J.S.T., S.M.S., N.C.G., J.S.P., K.W.D., A.H.E., A.L.K., and S.J.H. S.J.H. is on the advisory board of Sequoia Vaccines Inc. S.J.H. is a cofounder of Fimbrion Therapeutics that is developing FimH targeted therapies and may financially benefit if the company is successful. A.L.K. is a member of the Scientific Advisory Board for Ancilia Bio and received funding from Artizan Bioscience for work unrelated to the current study. The Ellebedy laboratory received funding from Emergent BioSolutions, AbbVie, and Moderna that are unrelated to the data presented in the current study. A.H.E. has received consulting and speaking fees from InBios International, Fimbrion Therapeutics, RGAX, Mubadala Investment Company, Moderna, Pfizer, GSK, Danaher, Third Rock Ventures, Goldman Sachs, and Morgan Stanley and is the founder of ImmuneBio Consulting. A.J.S., J.S.T., and A.H.E. are recipients of a licensing agreement with Abbvie that is unrelated to the data presented in the current study. The other authors declare that they have no competing interests. **Data and materials availability:** Cryo-EM data and protein models are deposited in the PDB and EMDB with identification as follows: PDB 9CCS and EMDB EMD-45456 (2H04-FimH), PDB 9CCT and EMDB EMD-45457 (B7-FimH), PDB 9CCU and EMDB EMD-45458 (F7-FimH), and PDB 9CCW and EMDB EMD-45460 (2C07-FimH). The data for Figs. 1 (D and E), 3 (A to C), 4 (A and B), and 5 (B, C, D, G, and H) and figs. S8 to S10 are deposited at Zenodo (https://zenodo.org/, DOIs: https://doi.org/10.5281/zenodo.15068905 and https://doi.org/10.5281/zenodo.15061268). All other data needed to evaluate the conclusions in the paper are present in the paper and/or the Supplementary Materials. All materials, including mAbs, generated in this study can be provided by S.J.H. pending scientific review and a completed material transfer agreement. Requests for materials should be submitted to: hultgren@wustl.edu.

Submitted 23 January 2025
Accepted 16 May 2025
Published 20 June 2025
10.1126/sciadv.adw0698